LANGMUIR

Article

pubs.acs.org/Langmuir

Molecular Engineering of the Peptoid Nanosheet Hydrophobic Core

Ellen J. Robertson, Caroline Proulx, Jessica K. Su, Rita L. Garcia, Stan Yoo, Eric M. Nehls, Michael D. Connolly, Laudann Taravati, and Ronald N. Zuckermann*

Molecular Foundry, Lawrence Berkeley National Laboratory, 1 Cyclotron Road, Berkeley, California 94720, United States

Supporting Information

ABSTRACT: The relationship between the structure of sequence-defined peptoid polymers and their ability to assemble into well-defined nanostructures is important to the creation of new bioinspired platforms with sophisticated functionality. Here, the hydrophobic *N*-(2-phenylethyl)glycine (Npe) monomers of the standard nanosheet-forming peptoid sequence were modified in an effort to (1) produce nanosheets from relatively short peptoids, (2) inhibit the aggregation of peptoids in bulk solution, (3) increase nanosheet stability by promoting packing interactions within the hydrophobic core, and (4) produce nanosheets with a nonaromatic hydrophobic core. Fluorescence and optical microscopy of individual nanosheets reveal that certain modifications to the hydrophobic core were well tolerated, whereas others resulted in instability or aggregation or prevented assembly. Importantly, we demonstrate that substitution at the meta and para positions of the Npe aromatic ring are well tolerated, enabling significant opportunities to tune the functional properties of peptoid nanosheets. We also found that *N*-aryl glycine monomers inhibit nanosheet formation, whereas branched aliphatic monomers have the ability to form nanosheets. An analysis of the crystal structures of several *N*,*N*′-disubstituted diketopiperazines (DKPs), a simple model system, revealed that the preferred solid-state packing arrangement of the hydrophobic groups can directly inform the assembly of stable peptoid nanosheets.

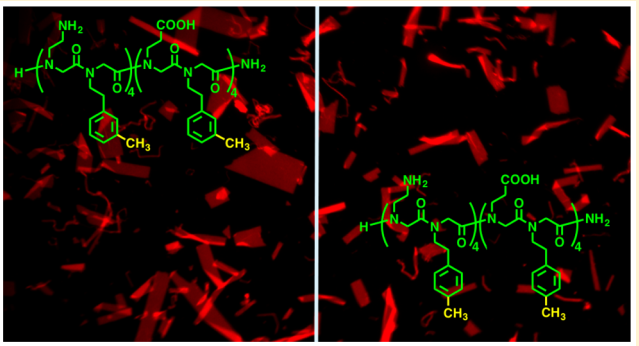

INTRODUCTION

There is increasing interest in polymer-based two-dimensional (2D) nanomaterials for use in sensing, catalysis, biomineralization, and drug delivery.[1−10] Peptoid polymers are sequence-defined peptide mimetics that show great promise for folding into a variety of different functional structures.[11−19] One recently discovered structure is the free-floating two-dimensional peptoid nanosheet.[20] These bilayer materials have been shown to self-assemble from amphiphilic peptoid strands that alternate between ionic and hydrophobic monomers in a 2-fold periodic sequence pattern via a unique monolayer collapse mechanism.[20] To employ peptoid nanosheets in a wider range of applications, molecular engineering of the nanosheet structure is needed to introduce a greater diversity of functional groups at precise locations. For example, to create antibody-like structures for molecular recognition, we demonstrated that hydrophilic peptoid and peptide domains could be inserted into the middle of a nanosheet-forming sequence, resulting in the formation of displayed loops on the nanosheet surface.[21] In contrast, we also showed that the interior of the nanosheet structure could be modified by introducing photo-cross-linkable *N*-2-(4-chlorophenyl)ethyl)glycine monomers at every other hydrophobic position, allowing the convenient preparation of highly stable cross-linked nanosheets.[22] Ultimately, we seek to engineer non-natural nanostructures with the same structural precision associated with protein engineering.[23,24]

In the past, intuition has primarily guided our sequence design, where functional groups in the hydrophobic core were introduced at the para position of the *N*-2-(phenylethyl)glycine monomer in order to minimally disrupt packing interactions in the bilayer interior.[21,22] Recently, however, an atomistic model of the peptoid nanosheet was developed, revealing critical information about the unique secondary structure (Σ-strand) adopted by the peptoid strands embedded in the nanosheet as well as their interchain packing interactions.[25] This detailed atomistic model provides a better understanding of how the chains fit together and enables the rational design of second-generation peptoid nanosheets with improved properties, such as increased stability, specific binding, higher long-range order, photoresponsiveness, controlled porosity, and cargo delivery.

Here, we present the systematic synthesis of a series of amphiphilic peptoid analogs with varying hydrophobic monomers to establish a structure−assembly relationship. This allows the identification of chemical features of the nanosheet-forming sequences that can be modified without disrupting the supramolecular assembly pathway. Nanosheet formation was followed by fluorescence and differential interference contrast microscopy. The hydrophobicity and surface tension of each free peptoid were also determined in

Received: July 25, 2016
Revised: September 18, 2016

DOI: 10.1021/acs.langmuir.6b02735
Langmuir XXXX, XXX, XXX−XXX

order to understand the practical limits of the assembly process. Many cyclic dipeptoids bearing the hydrophobic monomers under study were also crystallized in order to further understand their preferred solid-state packing interactions. Taken together, this study provides essential insight into the engineerability of the peptoid nanosheet structure, enabling future studies based on this versatile 2D nanomaterial platform.

EXPERIMENTAL SECTION

Materials. Bromoacetic acid, *N*,*N*′-diisopropylcarbodiimide (DIC), trifluoroacetic acid, triisopropylsilyl ether (TIPS), and all amine reagents were purchased from commercial sources and used without further purification. Solvents were purchased from commercial sources.

Peptoid Synthesis and Purification. Peptoids **1**−**3** and **5**−**18** were synthesized on polystyrene Rink amide resin (0.57 mmol/g) using either a Prelude or Aapptec automated peptide synthesizer and the solid-phase submonomer peptoid synthesis procedure, according to previously described methods.[21,22] The peptoids were cleaved from the resin using 95:2.5:2.5 TFA/H_2O/TIPS (v/v/v). The volatiles were removed using a Biotage V-10 evaporator to afford the crude peptoids, which were redissolved in a mixture of acetonitrile and water (1:1, v/v) and purified by reverse-phase HPLC using a C18 semipreparative column (5 μm, 250 mm × 21.2 mm, C18 Vydac column) with a flow rate of 15 mL/min. The collected fractions were concentrated and lyophilized to afford the purified peptoids as white, fluffy powders. Peptoid **4** was synthesized on polystyrene Rink amide resin (0.57 mmol/g) in a filtration tube equipped with a cap and stopcock using previously established conditions for the addition of aniline submonomers.[26]

Analytical HPLC analyses were performed on a 5 μm, 150 mm × 4.6 mm C18 Vydac column at 60 °C with a flow rate of 1.0 mL/min. HPLC traces were monitored at 214 nm. The retention times from analytical HPLC are reported here as a metric for peptoid hydrophobicity. The calculated octanol/water partition coefficients (cLogP) for the monomers were obtained using the Molinspiration Property Calculation Service.[27]

Nanosheet Preparation and Characterization. Nanosheets were prepared using the previously reported vial rocking method[28] under the standard nanosheet-forming conditions. These conditions consist of preparing nanosheet-forming solutions from 2 mM stock solutions of pure, lyophilized peptoid dissolved in 2:1 DMSO/water (v/v). The peptoid stock solutions were diluted to 20 μM in 10 mM Tris buffer at pH 8. Using a custom-built vial rocker, 2 mL glass vials containing the peptoid solutions were held horizontal for 900 s to allow peptoid adsorption to the air−water interface. After the 900 s wait time, the vials were rotated to the vertical position, causing a decrease in the air−water surface area that is required for monolayer collapse and peptoid nanosheet formation. This rocking procedure was repeated for ∼180 cycles (∼2 days of rocking).

After rocking, nanosheet solutions were imaged using fluorescence microscopy as previously reported.[22] Briefly, 2 μL of the nanosheet solution was incubated with 0.5 μM Nile red for 30 min and then transferred to a 1% porous agarose gel pad. Nile red is an environmentally sensitive dye whose fluorescence intensity increases in hydrophobic environments and so stains the nanosheet hydrophobic core. The nanosheets were imaged under epifluorescence illumination using an Olympus IX81 inverted microscope fitted with a Hamamatsu Orca CCD camera. Optical images of the nanosheets were also obtained on the 1% agar gels on a Leica DM4000 optical microscope using differential interference contrast (DIC).

Surface Pressure Measurements. Surface pressure measurements were obtained using a Theta optical tensiometer (OneAttension, Biolin Scientific). Here, an ∼10 μL drop containing the peptoid (20 μM peptoid, 10 mM Tris buffer, pH 8) was suspended from a 1 mL Gastight Hamilton syringe fitted with an 18 gauge blunt needle that had been copiously washed with ethanol and water from a Milli-Q filtration system (18.2 MΩ cm^{-1}). The cleanliness of the syringe−needle system was ensured before measuring the peptoid solution by producing a neat air−water surface tension of ∼72 mN/m. The volume of the drop was controlled using an automated liquid dispenser from Biolin Scientific. The hanging droplet was surrounded by a cuvette with a septum cap in order to prevent droplet evaporation over time. Images of the droplet were collected using a Gigabit Ethernet camera (76 frames/s at 782 × 582 resolution) at a rate of at least 0.1 frames/s for 900 s. The drop shape was fit to the Laplace−Young equation using OneAttension software to obtain the shape factor, β, which was then used in eq 1 to determine the surface tension, γ.[29]

$$\gamma = \frac{\Delta\rho g b}{\beta} \tag{1}$$

Here, $\Delta\rho$ is the density difference between the two phases, g is the gravitational constant, and b is the radius at the drop apex. We report the surface pressure, which is given as the difference between the surface tension of the air−10 mM Tris (pH 8) interface (∼72 mN/m) and the surface tension of the peptoid solution. The reported surface pressure values are of the peptoid monolayers recorded 900 s after the formation of the air−aqueous peptoid solution interface (SP_{900}). The surface pressure vs time traces are an average from at least three measurements made using the pendant drop tensiometer and one measurement from peptoid solutions in a Langmuir trough (Mini-trough, KSV Nima) using the Wilhelmy plate method, as previously described.[21,28]

Cyclic Dipeptoid Synthesis and Crystallization. *N*,*N*′-Disubstituted diketopiperazines[30] (DKPs) functionalized with methyl phenylethyl analogs were synthesized by cyclizing the relevant peptoid dimer C-terminal acids. To synthesize the dimers, manual solid-phase synthesis was performed via the submonomer method on 2-chlorotrityl chloride resin.[31] The peptoids were cleaved from the resin with 5% trifluoroacetic acid in dichloromethane (4 mL), redissolved in ethanol (6 mL), and cyclized overnight at 60 °C. The crude products were identified by liquid chromatography−mass spectrometry (LC−MS) and then concentrated and purified by recrystallization. Specifically, the DKPs were recrystallized by vapor diffusion: 10−20 mg of crude material was dissolved in dichloromethane (∼200 μL) to make a concentrated solution in a 1 mL vial, which was placed inside a 20 mL scintillation vial containing 2 mL of acetonitrile and allowed to equilibrate to promote crystal growth. Crystal structures were determined at UC Berkeley's Small Molecule X-ray Crystallography Facility.

RESULTS AND DISCUSSION

Nanosheet formation proceeds via a unique monolayer collapse mechanism at the air−water interface.[28] Previous studies have demonstrated that stable nanosheets form from amphiphilic peptoids in which hydrophobic (aromatic) and polar (ionic) monomers alternate with 2-fold periodicity. For the standard 28-residue nanosheet-forming peptoid[20] (peptoid **14**), the hydrophobic monomers consist of *N*-(2-phenylethyl)glycines (Npe) and the ionic monomers consist of *N*-(2-aminoethyl)-glycines (Nae) and *N*-(2-carboxyethyl)glycines (Nce) arranged in block-charge domains. Keeping with this amphiphilic block-charge architecture, a series of peptoid analogues were synthesized in which some or all of the hydrophobic Npe monomers were replaced in order to probe the limits of nanosheet assembly.

All peptoid analogues were tested for nanosheet assembly under a standard set of conditions in which a 20 μM solution of peptoid (in 10 mM Tris at pH 8) was allowed to sit for 900 s for monolayer assembly prior to surface compression. Because nanosheet assembly occurs via monolayer collapse, it is necessary that the peptoid analogues adsorb effectively to the air−water interface before monolayer compression. Each peptoid therefore must possess a proper balance between hydrophobicity (to enhance peptoid adsorption) and solubility

DOI: 10.1021/acs.langmuir.6b02735
Langmuir XXXX, XXX, XXX−XXX

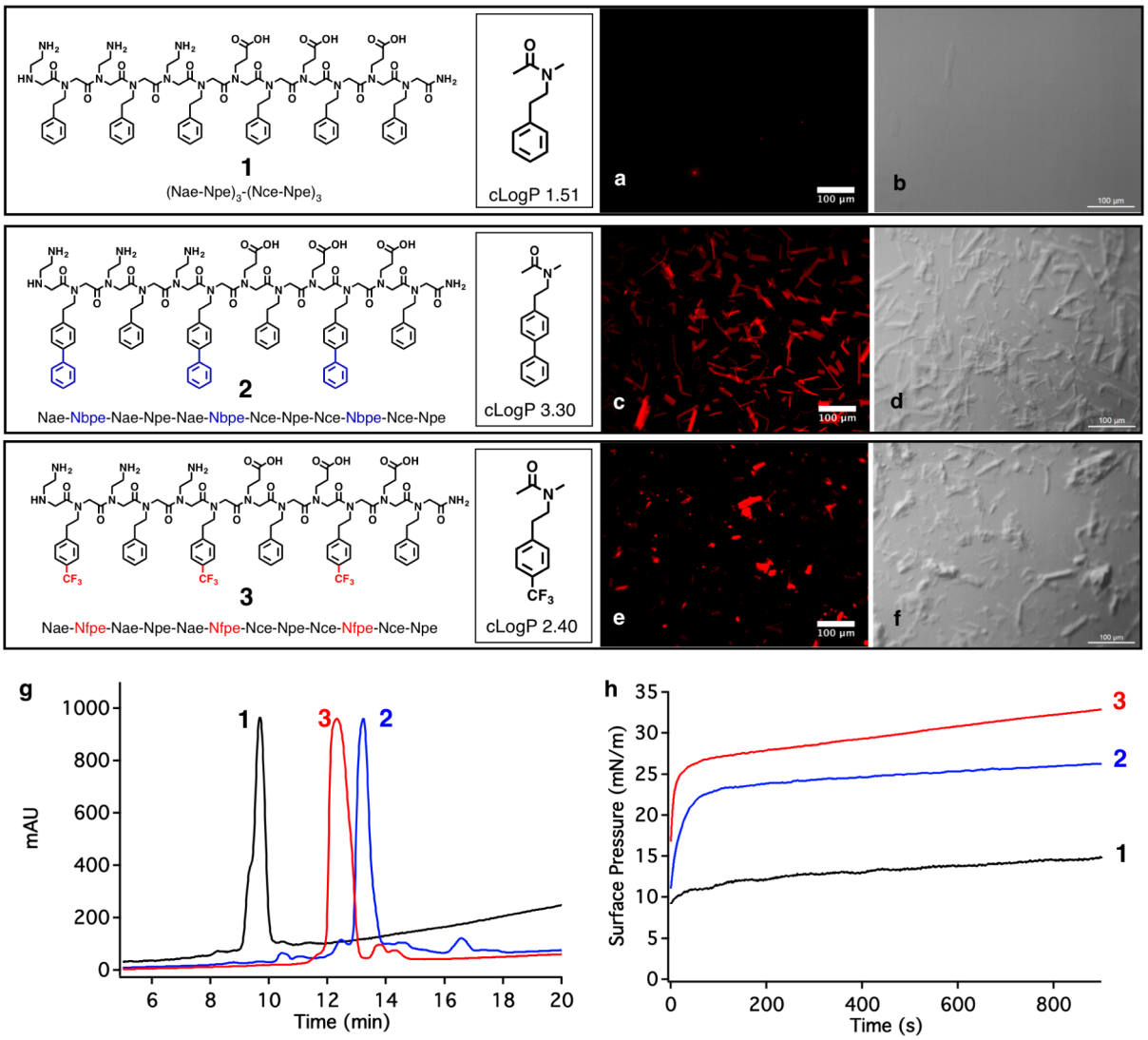

Figure 1. Chemical structures of the peptoid dodecamer analogues with corresponding cLogP values for the hydrophobic monomers and their properties. Nile red fluorescence (a, c, and e) and DIC (b, d, and f) microscopy images for solutions of peptoids **1**, **2**, and **3**, respectively, that had been rocked under the standard nanosheet-forming conditions. (g) Relative peptoid hydrophobicities as determined by retention times on reverse-phase analytical HPLC for purified peptoids **1** (black), **2** (blue), and **3** (red). (h) Surface pressure as a function of time for peptoids **1** (black), **2** (blue), and **3** (red).

(to avoid aggregation in bulk solution). We therefore assessed the relative degrees of peptoid hydrophobicity by comparing both the calculated octanol/water partition coefficient (cLogP)[27] for each hydrophobic monomer and the retention time for each peptoid from reverse-phase analytical HPLC. To assess the degree of monolayer assembly at the time of compression, we report the surface pressure values for all peptoid monolayers after a freshly prepared solution had been left undisturbed for a wait time of 900 s (SP_{900}). Although not all peptoids reached their equilibrium surface pressure values at 900 s, by this time the surface pressure values for all peptoids were stable (i.e., not changing more than 5 mN/m in 10 min). We therefore determined that 900 s was an appropriate amount of time to allow for monolayer formation to occur, although some peptoid monolayers are capable of collapse in a much shorter amount of time. The SP_{900} values and HPLC retention times are listed in Table S1. In addition, all peptoid solutions were checked for solution aggregation to determine if they were above or below the critical aggregation concentration. Optical microscopy images of undisturbed peptoid solutions after 2.5 days reveal the presence or absence of aggregates formed from bulk solution (Figure S6). Peptoid analogues were considered successful if nanosheets formed under the standard conditions in a higher yield than aggregates formed in bulk solution.

Increasing Aromatic Interactions in 12mers. In an effort to identify the most synthetically accessible nanosheet-forming peptoid sequences, we focused on enhancing the chemical structure of the shortest peptoids known to assemble (dodecamers). By keeping the main chain short, synthesis times are reduced and higher crude purities can be obtained, lessening the demand for purification. Previous studies have shown that the 12-residue peptoid, $(Nae\text{-}Npe)_3\text{-}(Nce\text{-}Npe)_3$ (Figure 1, peptoid **1**), is the shortest block-charge peptoid capable of forming nanosheets with the standard hydrophobic Npe monomer.[25] However, these nanosheets were not formed under the standard conditions, requiring instead a 50-fold increase in the bulk peptoid concentration to produce a

DOI: 10.1021/acs.langmuir.6b02735
Langmuir XXXX, XXX, XXX−XXX

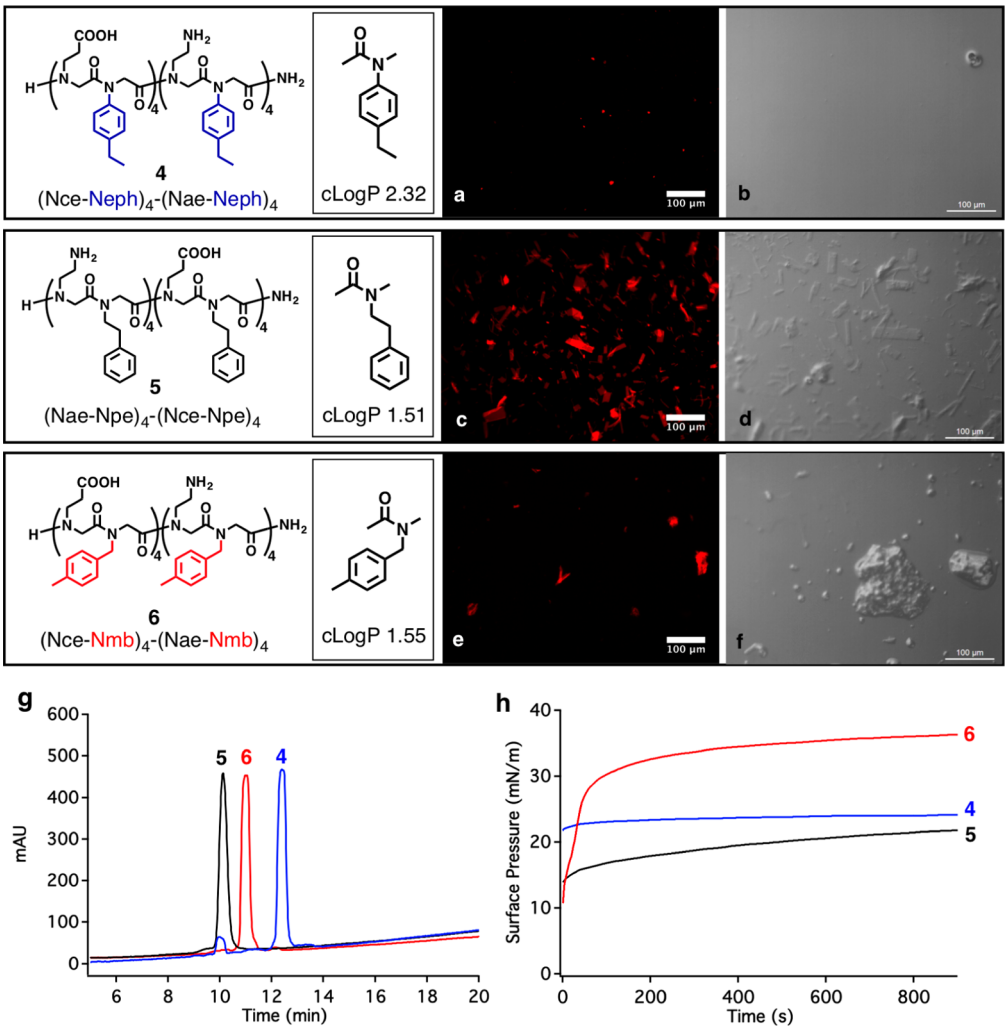

Figure 2. Chemical structures of the 16-residue peptoid analogues in which the aromatic side chain length has been varied, with corresponding cLogP values for the hydrophobic monomers, relative peptoid hydrophobicities, surface activities, and nanosheet-forming abilities. Fluorescence (a, c, and e) and DIC (b, d, and f) microscopy images for solutions of peptoids **4**, **5**, and **6**, respectively, that had been rocked under the standard nanosheet-forming conditions. (g) Reverse-phase analytical HPLC traces for purified peptoids **4** (blue), **2** (black), and **6** (red). (h) Surface pressure as a function of time for peptoids **4** (blue), **5** (black), and **6** (red).

monolayer capable of collapse into nanosheets. Moreover, these nanosheets were unstable in solution over time.

We reasoned that increasing the degree of hydrophobic interactions within the nanosheet core should enhance the stability of nanosheets. This is essential for forming nanosheets from 12mers under the standard nanosheet-forming conditions. To this end, we added either *N*-2-((4-biphenyl)ethyl)glycine (Nbpe) or *N*-2-(4-(trifluoromethyl)phenylethyl)glycine (Nfpe) to every other hydrophobic position of peptoid **1**, resulting in peptoids **2** and **3**, respectively (Figure 1). Both Nbpe and Nfpe are derived from commercially available submonomers and are significantly more hydrophobic than Npe, as seen from the calculated octanol/water partition coefficients (cLogP) for each monomer (Figure 1). Moreover, these analogues can enhance intermolecular $\pi-\pi$ interactions within the nanosheet core. The introduction of the Nbpe monomers into peptoid **2** increases the total number of aromatic rings per chain from six to nine. This monomer has previously been used to make nanosheets with very hydrophilic functional loop inserts to promote interfacial adsorption, monolayer formation, and nanosheet assembly.[21] Peptoid **3** has the advantage of rendering every other aromatic ring electron-poor, thus enhancing the degree of aromatic interactions between substituted and unsubstituted phenylethyl groups.

Unlike peptoid **1** (Figure 1a,b), both peptoids **2** (Figure 1c,d) and **3** (Figure 1e,f) successfully form nanosheets under the standard conditions, as seen in the fluorescence and DIC microscopy images. From the HPLC data (Figure 1g), the retention times of **2** (13.2 min) and **3** (12.3 min) are significantly longer than for **1** (9.7 min), indicating that, as expected, **2** and **3** are more hydrophobic than **1**. These data are consistent with the cLogP values for the hydrophobic Npe (1.51), Nbpe (3.30), and Nfpe (2.40) monomers. Because of this increase in hydrophobicity, one would expect reduced water solubility as well as enhanced adsorption of **2** and **3** at the interface. This was confirmed as indicated by surface pressure vs time data (Figure 1h). This enhanced adsorption is important for forming a sufficiently dense monolayer that is capable of collapse into bilayer nanosheets. Specifically, the SP_{900} values of **2** (26.2 ± 1.9 mN/m) and **3** (32.9 ± 2.4 mN/m) are significantly higher than that of **1** (14.8 ± 3.2 mN/m), indicating that **2** and **3** are more surface-active than **1**. Previous studies have shown that the surface activity of **1** can be increased when the peptoid bulk concentration is increased to 1

DOI: 10.1021/acs.langmuir.6b02735
Langmuir XXXX, XXX, XXX−XXX

mM, resulting in a surface pressure of 18.9 ± 1.4 mN/m under similar conditions.[25] Nanosheets were formed from these solutions, yet these nanosheets were unstable and degraded over the course of 1 week.

Although **2** and **3** both successfully assemble into nanosheets, it is clear from the microscopy images that with **3** (Figure 1e,f) there are large aggregates in addition to nanosheets. The appearance of these aggregates indicates that **3** is above its critical aggregation concentration under the standard nanosheet-forming conditions. This is not surprising, as the SP_{900} value of **3** is significantly higher than that of either **1** or **2**, showing its high propensity for accumulation at the interface. At this bulk peptoid concentration, the surface may have reached its maximum threshold for adsorption such that aggregation in bulk solution begins.[32] Aggregates, however, are not seen in the images of **2** (Figure 1c,d) despite its longer retention time when compared to that of **3**. Optical microscopy images of the corresponding unrocked peptoid solutions show that spontaneous aggregation in bulk solution occurs for both peptoids **2** and **3**. Thus, for peptoid **2** the formation of aggregates is slow enough to not interfere with nanosheet formation, whereas for peptoid **3** aggregation occurs at a fast enough rate to interfere with nanosheet formation. Moreover, stability studies of nanosheets composed of **2** or **3** have shown that whereas the **2** nanosheets remain intact in solution over the course of 1 week the **3** nanosheets begin to decompose into large aggregates (Figure S7). This indicates that aggregates composed of **3** are more stable than the corresponding nanosheets. This result is similar to what is seen for the nanosheets composed of **1** that were formed at a concentration of 1 mM.[25]

The nanosheets made from peptoid **2** are overall smaller and skinnier than those made from block charge peptoids containing the Npe monomer with 16 or 28 residues.[25] Recent atomic computer simulations of the Npe-containing nanosheets have shown that there are unfavorable interactions at the termini of each chain. Therefore, the shorter the peptoid chain, the higher the density of these chain−chain junctions, resulting in instability. Despite the smaller size of the **2** nanosheets, they remained stable in solution over the course of 1 week (Figure S7). Peptoid **2** is thus the shortest sequence that can form stable nanosheets and can be made from all commercially available submonomers.

Aromatic Side Chain Length. Atomistic simulations have shown that the stability and 2D flatness of peptoid nanosheets is attained through extended peptoid chains that adopt a unique secondary structure.[25] In this structure, called the Σ strand, the polymer backbone adopts binary rotational states, resulting in linear, twist-free peptoid chains within the nanosheet. To promote this extended secondary structure and thus improve the stability of the nanosheet, we incorporated hydrophobic monomers into the peptoid that are known to favor a trans backbone configuration ($\omega \approx 180°$).[16] *N*-Aryl glycines have been shown to strongly favor trans backbone amides in a study of short peptoid oligomers.[16] Here we used *N*-(4-ethylphenyl)-glycine (Neph) as the hydrophobic monomer in the synthesis of $(Nce\text{-}Neph)_4(Nae\text{-}Neph)_4$ (Figure 2, peptoid **4**), which provides the *N*-aryl component in addition to a pendant *p*-ethyl chain to preserve the same number of atoms as in the parent Npe monomer. Moreover, the Ramanchandren plot of *N*-methyl-*N*-phenyl-2-(*N*-phenylacetamido)acetamide[16] shows an energy minimum near one of minima exhibited by the Σ strand, further suggesting that the incorporation of the Neph monomer at every other position of the hydrophobic core has the potential to promote the Σ strand secondary structure in addition to favoring the trans amide configuration. However, the side-chain dihedral angle, χ, in *N*-phenylglycine residues is restricted to ∼90°, with the phenyl ring perpendicular to the plane of the amide bond, which might prevent productive interchain interactions. Peptoid **4** was synthesized with only 16 residues because this is just above the minimum size limit for forming stable nanosheets, allowing small differences in nanosheet stability due to specific modifications to be more easily differentiated than in larger peptoids. To serve as a comparison to **4**, the previously reported[25] 16-residue block charge peptoid with standard nanosheet-forming monomers $(Nae\text{-}Npe)_4\text{-}(Nce\text{-}Npe)_4$ was also characterized (Figure 2, peptoid **5**).

The atomistic simulations previously discussed have shown that the aromatic residues within the nanosheet hydrophobic core are relatively fluid due to the overall flexibility of the Npe monomer.[25] Moving the aromatic ring directly to the peptoid backbone, as with the Neph monomer, is likely to significantly inhibit the fluidity of the nanosheet core. We therefore made *N*-benzyl analogue **6** $(Nce\text{-}Nmb)_4\text{-}(Nae\text{-}Nmb)_4$, using *N*-(4-methylbenzyl)glycine (Nmb), to gain a deeper understanding of the effect of side-chain flexibility in the hydrophobic core (Figure 2). It was previously shown that *N*-benzylglycine (Nbe) could produce nanosheets, but in a lower yield than for those with the Npe monomer.[33] Peptoid **6** thus serves as a good comparison to **5**, in which the Npe side chain is relatively flexible, and to **4**, in which the Neph side chain is relatively inflexible. In all cases, the total number of carbon atoms remained unchanged to maintain the overall hydrophobicity of the peptoids in a similar range. Specifically, as the number of carbons decreased between the backbone nitrogen and phenyl ring, additional carbon atoms were added at the para position of the aromatic ring to compensate.

Changing the distance between the aromatic side chain and the backbone had a drastic effect on the ability of 16-residue peptoids to assemble into nanosheets. As seen in the fluorescence and DIC microscopy images, **4** shows the absence of both nanosheets and large aggregates (Figure 2a,b), **5** assembles into nanosheets (Figure 2c,d), and **6** produces some sheets and a large percentage of aggregates (Figure 2e,f). That **4** remains soluble in bulk solution under the standard nanosheet-forming conditions and does not form nanosheets is in contrast to what would be expected on the basis of its relative degrees of hydrophobicity and adsorption to the air−water interface when compared to the properties of peptoids **5** and **6**.

Changing the position of the aromatic ring with respect to the peptoid backbone changes the overall hydrophobicity of the peptoid as evidenced by the cLogP values for the hydrophobic monomers and the reverse-phase HPLC retention times of the peptoids. Here, the cLogP value of the Neph monomer (2.32) is much higher than that of either the Npe (1.51) or the Nmb (1.55) monomer. Moreover, Figure 2g shows that the retention time of peptoid **4** (12.4 min) is longer than that of either **5** (10.1 min) or **6** (11.0 min). Although these metrics indicate that **4** is the most hydrophobic of this peptoid series, they do not provide information on the behavior of the peptoids under the standard nanosheet-forming conditions (i.e., in aqueous solution at pH 8). Under those conditions, peptoid **4** is below its critical aggregation concentration.

The inability of **4** to form nanosheets from monolayer collapse is not due to its ability to adsorb to the air−water

DOI: 10.1021/acs.langmuir.6b02735
Langmuir XXXX, XXX, XXX−XXX

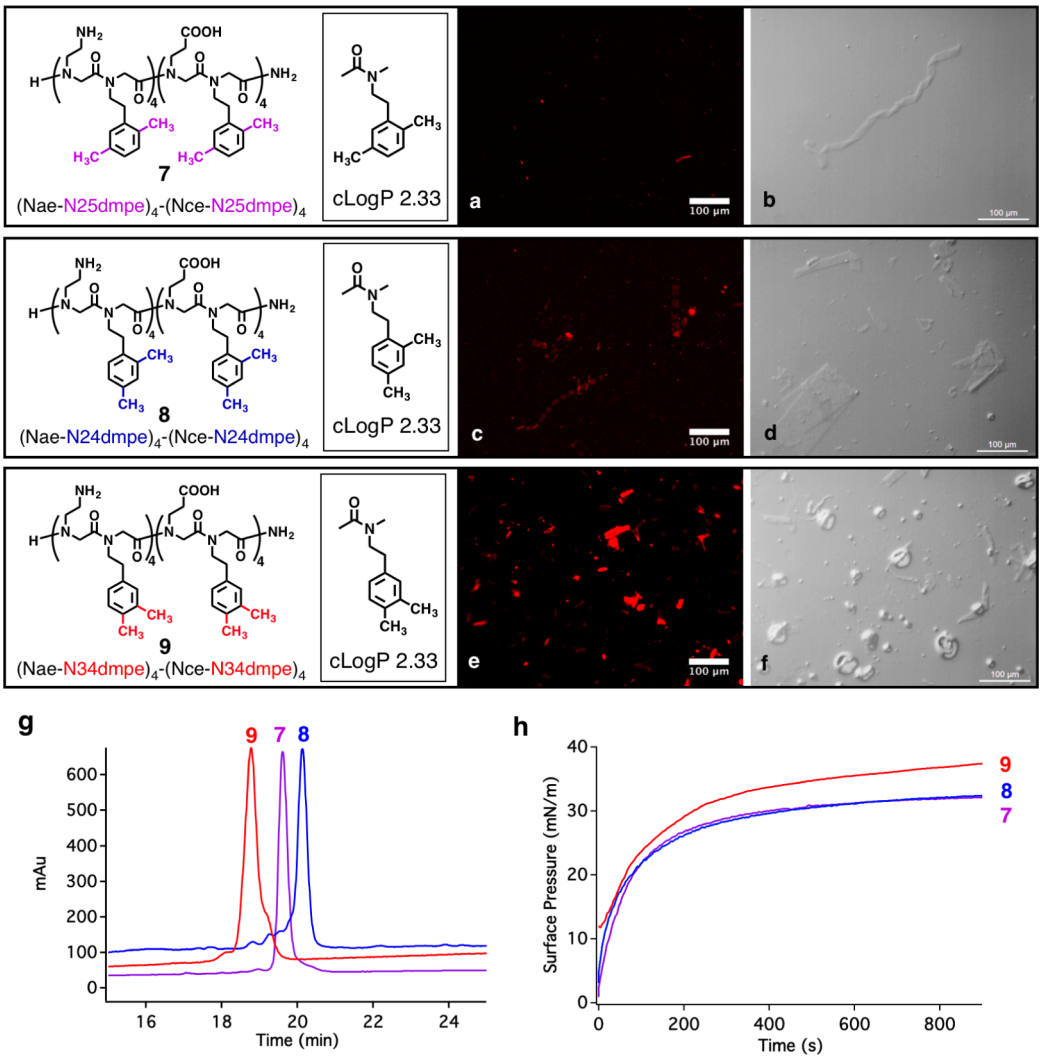

Figure 3. Chemical structures of the 16-residue peptoid analogues in which the aromatic rings of all Npe monomers are dimethyl-substituted, with corresponding cLogP values for the hydrophobic monomers, relative peptoid hydrophobicities, surface activities, and nanosheet-forming abilities. Fluorescence (a, c, and e) and DIC (b, d, and f) microscopy images for solutions of peptoids **7**, **8**, and **9**, respectively, that had been rocked under the standard nanosheet-forming conditions. (g) Reverse-phase analytical HPLC traces for purified peptoids **7** (purple), **8** (blue), and **9** (red). (h) Surface pressure as a function of time for peptoids **7** (purple), **8** (blue), and **9** (red).

interface, as shown by the surface pressure vs time data (Figure 2h). Here, the SP_{900} value of **4** (24.2 ± 1.7 mN/m) is not significantly different than that of the standard nanosheet-forming 16mer, **5** (21.8 ± 3.3 mN/m). The lack of nanosheet formation from **4** must therefore be due to the short residence time of the peptoid within the **4** monolayer that prevents monolayer collapse.[34] This was borne out in a detailed rheological study of these compounds, which reveals the importance of the monolayer residence time as well as other viscoelastic properties.[34]

For peptoid **6**, in which the aromatic ring is one carbon farther from the backbone as compared to **4**, the ability to form nanosheets is recovered. However, the aggregates in solution far outnumber the nanosheets. These aggregates form in bulk solution, as confirmed by the optical microscopy images of the corresponding unrocked solutions of peptoid **6** (Figure S6). According to the cLogP values of the monomers and peptoid retention times, **6** is far less hydrophobic than **4**. However, the distinctly large difference in the SP_{900} value (Figure 2h) between **4** (24.2 ± 1.7 mN/m) and **6** (36.3 ± 3.6 mN/m) shows that **6** more readily accumulates at the interface than **4**, consistent with the fact that **6** is above its critical aggregation concentration but **4** is not.

In this series, peptoid **5** is the least hydrophobic and adsorbs to the air−water interface to the least extent. That peptoid **5** forms only nanosheets and not aggregates (Figure S6) indicates that it is hydrophobic enough to adsorb to the air−water interface to a degree necessary for forming a collapsible monolayer yet is not so hydrophobic as to be above its critical aggregation concentration. Thus, positioning the aromatic ring no closer than two carbons from the peptoid backbone is optimal for nanosheet-forming peptoids. This result is consistent with atomistic computer simulations, which have noted the importance of the conformational flexibility of the side chains within the nanosheet.[25]

Positioning of Aromatic Substituents. One of the most straightforward ways to impart new functionality into the hydrophobic core of the nanosheet is to add functional substituents to the aromatic ring of the Npe monomer. This takes advantage of the fact that large numbers of substituted 2-phenylethylamines are commercially available. For example, photoresponsive halogen groups on the aromatic ring have

DOI: 10.1021/acs.langmuir.6b02735
Langmuir XXXX, XXX, XXX−XXX

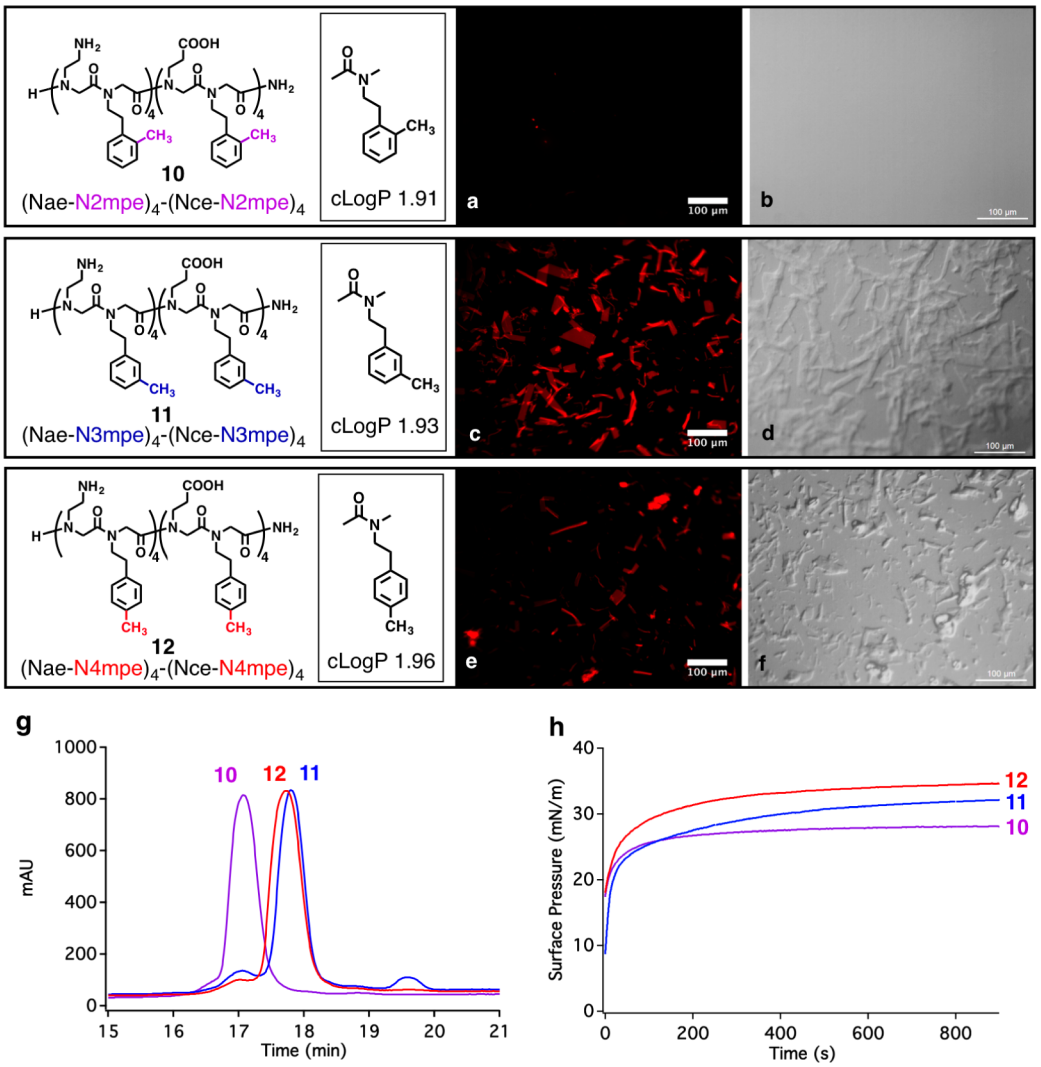

Figure 4. Chemical structures of the 16-residue peptoid analogues in which the aromatic rings of all Npe monomers are substituted with a single methyl group, with corresponding monomer cLogP values, relative peptoid hydrophobicities, surface activities, and nanosheet-forming abilities. Fluorescence (a, c, and e) and DIC (b, d, and f) microscopy images for solutions of peptoids **10**, **11**, and **12**, respectively, that had been rocked under the standard nanosheet-forming conditions. (g) Reverse-phase analytical HPLC traces for purified peptoids **10** (purple), **11** (blue), and **12** (red). (h) Surface pressure as a function of time for peptoids **10** (purple), **11** (blue), and **12** (red).

been used to cross-link the nanosheet hydrophobic core.[22] Recent MD simulations of the peptoid nanosheets have shown that there should be space for aromatic substitution within the nanosheet core. Specifically, the simulations show that the 2-phenylethyl groups are not crystalline and possess a degree of disorder within the nanosheet core, leaving a significant amount of room between aromatic side chains.[25] This property is supported by XRD spectra of peptoid nanosheets, in which relatively broad aromatic packing peaks indicate a significant degree of disorder within the nanosheet core.[20] The simulations also suggest that aromatic substitution could enhance the nanosheet stability by promoting a greater degree of packing within the nanosheet core. To systematically test the tolerance of nanosheet formation to aromatic substitution, we synthesized a series of 16mer peptoids in which all of the hydrophobic Npe monomers were either monomethyl (Nmpe)- or dimethyl (Ndmpe)-substituted.

The positioning of two methyl groups on the aromatic ring was first attempted to maximize the space occupied by the substituted Npe monomer. It was observed among three dimethyl-substituted analogues studied that whenever one of the methyl groups was in the ortho position it either inhibited nanosheet formation or resulted in nanosheets that were unstable in solution over the course of 1 week. Specifically, a peptoid with methyl substituents on both the ortho and meta positions ($(Nae\text{-}N25dmpe)_4$-$(Nce\text{-}N25dmpe)_4$, peptoid **7**) barely showed the presence of nanosheets in the microscopy images (Figure 3a,b). Even though nanosheets (Figure 3c,d) assembled from peptoids with both ortho and para substituents on the aromatic ring ($(Nae\text{-}N24dmpe)_4$-$(Nce\text{-}N24dmpe)_4$, peptoid **8**), they were unstable and degraded over the course of 1 week (Figure S7). Stable nanosheets formed only when both the meta and para positions of the aromatic ring were substituted with methyl groups ($(Nae\text{-}N34dmpe)_4$-$(Nce\text{-}N34dmpe)_4$, peptoid **9**), yet a large number of aggregates were also seen in these solutions (Figure 3e,f). Optical microscopy images of the corresponding unrocked solutions (Figure S6) show that aggregation occurs in bulk solution over time, indicating that **9** is above its critical aggregation concentration.

DOI: 10.1021/acs.langmuir.6b02735
Langmuir XXXX, XXX, XXX−XXX

The bulk aggregation behavior of the peptoids with dimethyl substitution does not correlate with the relative degree of peptoid hydrophobicity, as given by the monomer cLogP values or the peptoid retention times. The cLogP values for all dimethyl-substituted monomers are the same (2.33), indicating that these monomers have the same relative degree of hydrophobicity. The retention times, however, show that the peptoids have differing relative degrees of hydrophobicity. On the basis of these retention times (Figure 3g), **9** (18.8 min) is less hydrophobic than either **7** (19.6 min) or **8** (20.1 min). From the surface pressure data (Figure 3h), the least hydrophobic peptoid in this series is the most surface-active. Specifically, the SP_{900} values show that peptoid **9** (37.4 ± 1.4 mN/m) is significantly more surface-active than either **7** (32.1 ± 2.0 mN/m) or **8** (32.4 ± 2.6 mN/m). This high SP_{900} value for peptoid **9** is consistent with the fact that **9** is above its critical aggregation concentration. Thus, the SP_{900} value serves as a better indicator for peptoid aggregation under the standard nanosheet-forming conditions than the relative degree of peptoid hydrophobicity.

Because none of the dimethyl-substituted aromatic rings exhibited improved assemblies, we next examined monomethyl-substituted rings. The positioning of a single methyl substituent on the aromatic ring significantly impacts nanosheet assembly. Specifically, ortho substitution ($(Nae\text{-}N2mpe)_4$-$(Nce\text{-}N2mpe)_4$, peptoid **10**) results in no assembled structures (Figure 4a,b), meta substitution ($(Nae\text{-}N3mpe)_4$-$(Nce\text{-}N3mpe)_4$, peptoid **11**) produced exclusively peptoid nanosheets (Figure 4c-d), and para substitution ($(Nae\text{-}N4mpe)_4$-$(Nce\text{-}N4mpe)_4$, peptoid **12**) produced both peptoid nanosheets and large aggregates (Figure 4e,f). These results are consistent with what was seen for the dimethyl-substituted analogues in which substitution at the ortho position significantly hindered the formation of stable nanosheets.

Among the three monomethyl-substituted aromatic monomers, the cLogP values of N2mpe (1.91), N3mpe (1.93), and N4mpe (1.96) are all very close (Figure 4). On the basis of the retention times (Figure 4g), **10** (17.1 min) is somewhat less hydrophobic than either **11** (17.8 min) or **12** (17.7 min). Additionally, the SP_{900} values (Figure 4h) show that **10** (28.1 ± 1.3 mN/m) is slightly less surface-active than either **11** (32.1 ± 2.5 mN/m) or **12** (34.6 ± 1.0). Even though **10** is the least hydrophobic and surface-active of the monomethyl-substituted aromatic peptoids, it is both more hydrophobic and surface-active than the standard sheet-forming 16mer (peptoid **5**). This indicates that, as for peptoid **4**, adsorption to the air−water interface is not sufficient for **10** to assemble into nanosheets. This result again points to the importance of the viscoelastic properties of the peptoids within the monolayer.[34] In a separate study, it was shown that the peptoid residence time in the monolayer is in fact a key predictor of the ability of a peptoid monolayer to successfully collapse into a nanosheet.[34]

That both **11** and **12** can form nanosheets shows that substitutions of the aromatic ring at the meta and para positions are tolerated. Specifically for methyl substitution, the meta position appears to be the most favorable, as **11** is below its critical aggregation concentration under the standard nanosheet-forming conditions but **12** is not. Nanosheet formation was also tolerated from a 28-residue peptoid ($(Nae\text{-}Nclpe\text{-}Nae\text{-}Npe)_3$-Nae-Nclpe-$(Nce\text{-}Npe\text{-}Nce\text{-}Nclpe)_3$-Nce-Npe, peptoid **13**) in which the para position of every other Npe monomer was substituted with chlorine (Figure 5a, Nclpe).[22] The introduction of Nclpe into peptoid **13** led to nanosheets with

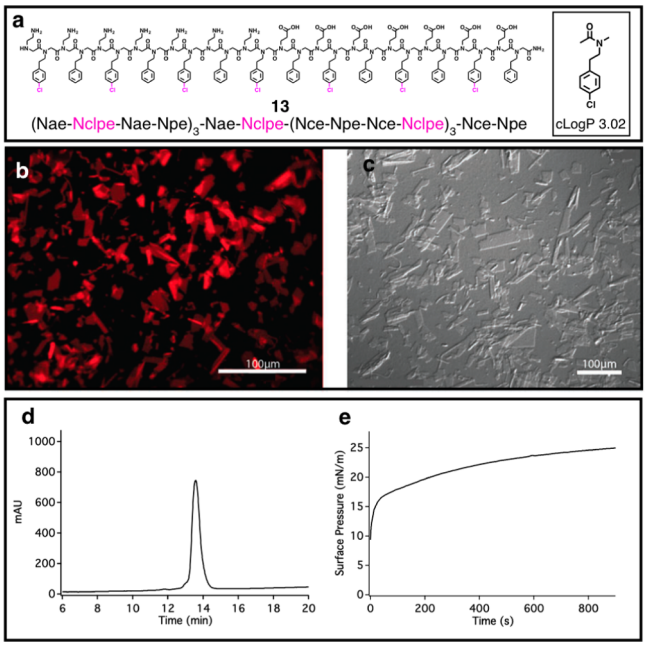

Figure 5. (a) Chemical structure of the 28-residue peptoid analogue in which the aromatic rings of every other Npe monomer is *para*-chloro substituted, with the corresponding cLogP value for the Nclpe monomer. (b) Fluorescence and (c) DIC microscopy images for solutions of peptoid **13** that had been rocked under the standard nanosheet-forming conditions. (d) Reverse-phase analytical HPLC trace and (e) surface pressure vs time data for peptoid **13**.

a functionalized hydrophobic core that could be photo-cross-linked to produce a nanosheet scaffold with enhanced stability.

As can be seen from the microscopy images of peptoid **13** (Figure 5b,c), nanosheets form during the rocking procedure, with no presence of aggregates. On the basis of the monomer cLogP values, the Nclpe monomer (3.02) is more hydrophobic than the N4mpe monomer. Even though the chain length of peptoid **13** is longer than that of peptoid **12**, the retention time of **13** (Figure 5d, 13.6 min) is less than that of **12**. Peptoid **13** is likely less hydrophobic than **12** because only half of the hydrophobic monomers are Nclpe. Moreover, peptoid **13** (Figure 5e, SP_{900} 25.0 ± 2.6 mN/m,) is less surface-active than **12**, which correlates with the fact that **13** is below its critical aggregation concentration but **12** is not.

The positioning of the aromatic substitution likely affects the aromatic packing interactions within the peptoid nanosheet hydrophobic core, which in turn can affect the nanosheet stability. To better understand these packing interactions between aryl monomers, we synthesized and crystallized a series of cyclic dipeptoids, or *N*,*N*′-disubstituted diketopiperazines[30] (DKPs), as models for the nanosheet hydrophobic core. The specific submonomers used in the synthesis of the DKPs are shown in Figure S8. The DKPs were synthesized by the cyclization of the corresponding linear dipeptoid C-terminal acid.[31] The crystal structures displaying the hydrophobic interfaces of several aromatic DKPs are shown in Figure 6. As seen here, most of the DKPs formed layered crystals, where all of the aromatic rings are packed within a plane as they would be within the core of a peptoid nanosheet.

The X-ray crystal structures of the DKPs were analyzed by looking at the packing behavior across several unit cells. From these data, the degree of lateral packing of the hydrophobic monomers was calculated as the cross-sectional area occupied

DOI: 10.1021/acs.langmuir.6b02735
Langmuir XXXX, XXX, XXX−XXX

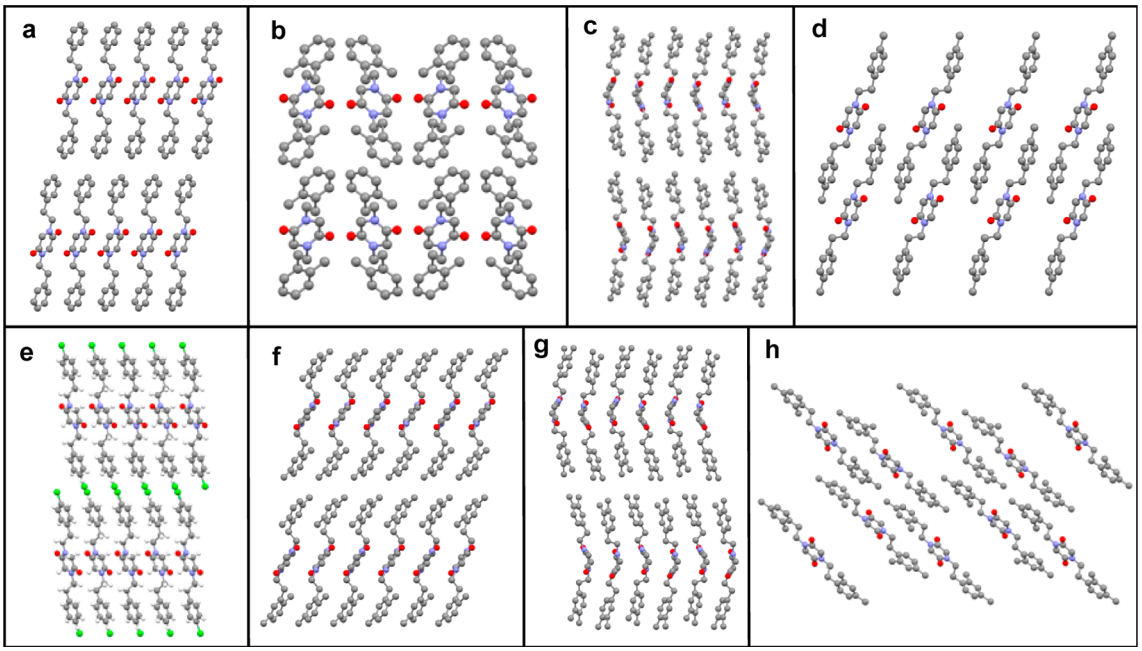

Figure 6. Crystal structures of various substituted aromatic *N*,*N*′-disubstituted diketopiperazines, including (a) *cyclo*-[Npe-Npe], (b) *cyclo*-[N2mpe-N2mpe], (c) *cyclo*-[N3mpe-N3mpe], (d) *cyclo*-[N4mpe-N4mpe], (e) *cyclo*-[Npe-Nclpe], (f) *cyclo*-[N25dmpe-N25dmpe], (g) *cyclo*-[N34dmpe-N34dmpe], and (h) *cyclo*-[N24dmpe-N24dmpe]. For all crystal structures except d and h, the crystal structures depict the planar faces of aromatic rings, as would be expected in a peptoid nanosheet.

by each DKP molecule within the crystal structure (Figure S8), as discussed in detail in the Supporting Information. The degree of packing for *cyclo*-[N24dmpe-N24dmpe] DKP (Figure 6h) was not calculated, as the packing within this crystal structure was not planar. For the standard sheet-forming Npe hydrophobic monomer (Figure 6a), the degree of packing was calculated to be 23.0 Å^2 per bis-*N*-2-phenylethyl DKP molecule. Adding one methyl substituent to the Npe monomer increased the lateral surface area occupied by each corresponding DKP molecule, albeit to different degrees depending upon the positioning on the aromatic ring. Specifically, the degree of packing for the *ortho*-methyl-substituted Npe was calculated to be 41.5 Å per *cyclo*-[N2mpe-N2mpe] DKP molecule (Figure 6b); for the *meta*-methyl-substituted Npe, it was calculated to be 24.3 Å^2 per *cyclo*-[N3mpe-N3mpe] DKP molecule (Figure 6c); and for the *para*-methyl-substituted Npe, it was determined to be 24.0 Å^2 per *cyclo*-[N4mpe-N4mpe] DKP molecule (Figure 6d). The lateral surface area determined from the *cyclo*-[Npe-Nclpe] DKP crystal structure (23.3 Å^2 per *cyclo*-[Npe-Nclpe] DKP molecule, Figure 6e) is between that of the unsubstituted Npe monomer and that of the *para*-methyl-substituted monomer. As can be seen, moving a methyl group closer to the amide backbone acts to disrupt the degree of packing of the monosubstituted Npe monomers, as is most evident when a methyl group is in the ortho position. This significant increase in surface area for the N2mpe monomer is likely due to steric effects. Adding a second methyl substituent to the Npe monomer has different effects depending upon the exact position on the aromatic ring. Interestingly, the lateral surface area of the N25dmpe monomer (27.8 Å^2 per *cyclo*-[N25dmpe-N25dmpe] DKP molecule, Figure 6f) is significantly less than that of the N2mpe monomer yet greater than that of the N3mpe monomer. However, the degree of packing of the N34dmpe monomer (24.8 Å^2 per *cyclo*-[N34dmpe-N34dmpe] DKP molecule, Figure 6g) is only slightly less than that of N3mpe and N4mpe. The extra methyl substituent at the meta position acts to overcome some of the steric effects that prevent a high degree of packing for the *ortho*-methyl-Npe monomer. This increased packing could possibly occur through enhanced hydrophobic interactions between the methyl groups at the meta position.

The lateral surface area per monomer obtained from representative DKP crystal structures serves as a relatively good metric for predicting whether a hydrophobic monomer will support nanosheet formation. As seen here, the DKP molecules corresponding to hydrophobic monomers that were tolerated in nanosheet formation occupied less than 25 Å^2 in the crystal structure. The large monomer surface areas seen in both the N2mpe-N2mpe and N25dmpe-N25dmpe DKP crystal structures likely manifest during monolayer formation of the corresponding peptoids, as reflected by recent measurements of the peptoid monolayer residence time.[34] The relatively short residence times for peptoids **7** and **10** indicate that the chains are prevented from packing closely with one another during monolayer collapse into bilayer nanosheets.[34]

Aliphatic Core. All nanosheets previously published and presented so far here are based on aromatic hydrophobic monomers. Although recent MD simulations of the nanosheets have shown that aromatic interactions do promote stability,[25] it is unknown whether they are essential to forming stable nanosheets. Extending the hydrophobic monomer set to those with aliphatic groups has the potential to significantly alter the properties of the nanosheet hydrophobic core, creating new design opportunities. To probe the importance of aromatic interactions in the hydrophobic core, a series of 28mer peptoids were synthesized with aliphatic hydrophobic monomers of hydrophobicity comparable to that of the Npe monomer. Specifically, *N*-(cyclopentyl)glycine (Ncp), *N*-(cyclohexyl)-glycine (Nch), *N*-(*i*-butyl)glycine (Nibu), and *N*-(3-methylbutyl)glycine (N3mbu) were incorporated into the

DOI: 10.1021/acs.langmuir.6b02735
Langmuir XXXX, XXX, XXX−XXX

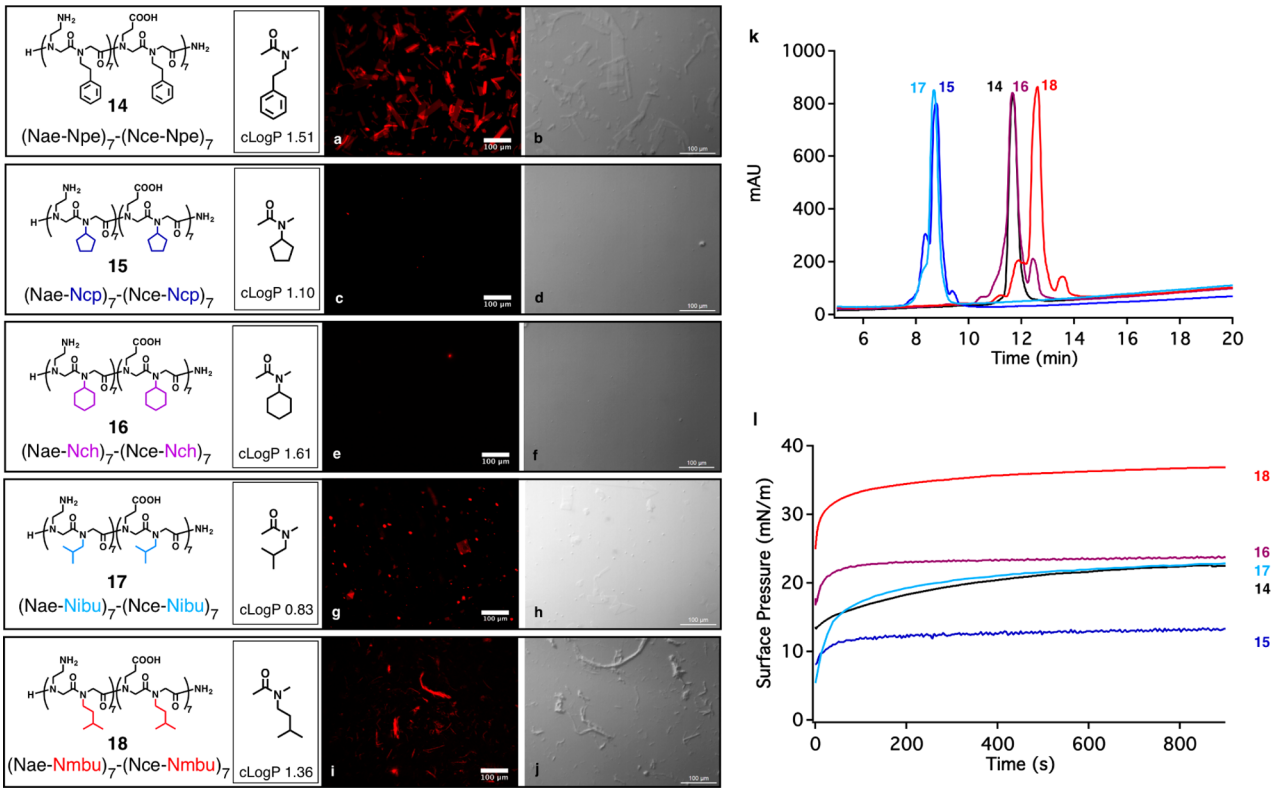

Figure 7. Chemical structures of the 28-residue peptoid analogues in which the hydrophobic monomers are aliphatic, with corresponding monomer cLogP values, relative peptoid hydrophobicities, surface activities, and nanosheet-forming abilities. Fluorescence (a, c, e, g, and i) and DIC (b, d, f, h, and j) microscopy images for solutions of peptoids **14**, **15**, **16**, **17**, and **18**, respectively, that had been rocked under the standard nanosheet-forming conditions. (k) Reverse-phase analytical HPLC traces for purified peptoids **14** (black), **15** (blue), **16** (maroon), **17** (light blue), and **18** (red). (l) Surface pressure as a function of time for peptoids **14** (black), **15** (blue), **16** (maroon), **17** (light blue), and **18** (red).

28mer design (Figure 7). The latter two analogues were inspired by biological systems. The Nibu and Nmbu monomers are close analogues of amino acids leucine and valine, respectively. These branched aliphatic amino acids significantly contribute to the stability of the well-known leucine zipper coiled-coil structure.[35] These specific peptoids were therefore designed to enhance hydrophobic and van der Waals interactions within the hydrophobic nanosheet core in a manner similar to the way in which valine and leucine promote the stability of leucine zippers.

The nanosheet-forming ability of the aliphatic peptoids were compared to that of the standard nanosheet-forming peptoid with 28 residues ($(Nae\text{-}Npe)_7$-$(Nce\text{-}Npe)_7$, peptoid **14**). As has been shown previously,[21] **14** assembles into nanosheets, showing an absence of large aggregates in the fluorescence and DIC microscopy images (Figure 7a,b). Nanosheets were not formed from the peptoids with cyclic aliphatic monomers Ncp ($(Nae\text{-}Ncp)_7$-$(Nce\text{-}Npe)_7$, peptoid **15**) or Nch ($(Nae\text{-}Nch)_7$-$(Nch\text{-}Npe)_7$, peptoid **16**) (Figure 7c–f). For peptoid **15**, the inability to form nanosheets may in part result from the fact that the Ncp monomer (Figure 7, cLogP 1.10) is less hydrophobic than the Npe monomer (Figure 7, cLogP 1.51). Moreover, the retention time of **15** (Figure 7k, 8.8 min) is significantly shorter than that of **14** (Figure 7k, 11.7 min), indicating that **15** is overall less hydrophobic than **14**. Most importantly, SP_{900} values (Figure 7l) show that **15** (13.3 ± 4.6 mN/m) is significantly less surface-active than **14** (22.5 ± 2.2). These results indicate that **15** may not be able to form a dense enough monolayer capable of collapse into nanosheets because it is not sufficiently hydrophobic. However, **16** is also unable to form nanosheets, and in this case, the Nch monomer (Figure 7, cLogP 1.61) is more hydrophobic than the Npe monomer. In fact, on the basis of the retention times (Figure 7k), peptoids **14** and **16** (11.7 min) have nearly identical relative hydrophobicities. The SP_{900} value for **16** (23.8 ± 3.1 mN/m) is also nearly identical to that of **14**, indicating a similar degree of adsorption to the air–water interface. Like peptoids **4**, **8**, and **11**, the degree of adsorption to the air–water interface and thus monolayer assembly are not sufficient for peptoid **16** to form nanosheets. For these cyclic hydrophobic monomers, the ring is directly attached to the backbone amide nitrogen and thus may act to reduce the flexibility of the backbone or restrict its conformation. Instead, rheology studies have recently shown that poor packing of these peptoid chains within the monolayer results in a rapid exchange with the peptoids subphase, which prevents monolayer collapse into bilayer nanosheets.[34]

Interestingly, nanosheets were formed from the peptoids with branched aliphatic monomers Nibu ($(Nae\text{-}Nibu)_7$-$(Nce\text{-}Nibu)_7$, peptoid **17**) and Nmbu ($(Nae\text{-}Nmbu)_7$-$(Nce\text{-}Nmbu)_7$, peptoid **18**) (Figure 7g–j). The peptoids formed from **18** were further characterized using X-ray diffraction (XRD), atomic force microscopy (AFM), and scanning electron microscopy (SEM), the results of which are shown in the Supporting Information (Figure S9–S11). The SEM images show that individual nanosheets composed of **18** are flat, having a morphology similar to that of nanosheets made from **14**.[20] However, the **18** nanosheets in the SEM images also show a tendency to stack on top of each other. This is also apparent in the optical microscopy images. AFM images show that individual **18** nanosheets are ~2.0 nm thick, which is ~1 nm

DOI: 10.1021/acs.langmuir.6b02735
Langmuir XXXX, XXX, XXX–XXX

thinner than what is observed in the AFM data of **14** nanosheets (3.0 nm). The XRD data confirm that the nanosheets composed of **18** are thinner than those composed of **14**, with the XRD spectrum of the **18** nanosheets showing a thickness peak at 2.4 nm compared to the 2.8 nm peak seen in the XRD spectrum of the **14** nanosheets.[20] This thickness difference is expected, as the Nmbu monomer is ∼2 Å shorter than the Npe monomer. Despite this difference in thickness between nanosheets composed of **14** and those composed of **18**, the XRD spectrum of nanosheets composed of **18** shows the same chain−chain spacing between peptoids (4.6 Å) as that seen for nanosheets composed of **14**,[20] as expected. One major difference between **14** and **18** is that **18** produces more aggregates in bulk solution than **14**, as seen in the optical microscopy images of the corresponding unrocked peptoid solutions (Figure S6). Although the Nmbu monomer (Figure 7, cLogP 1.36) is not as hydrophobic as the Npe monomer, the retention time of **18** (Figure 7k, 12.6 min) is longer than that of **14**. Moreover, the SP_{900} value for **18** (Figure 7l, 36.9 ± 1.4 mN/m) is significantly higher than for **14**, consistent with the fact that **18** is above its critical aggregation concentration under the standard nanosheet-forming conditions but **14** is not.

Extensive characterization was not performed on nanosheets composed of **17**, as these nanosheets were not stable enough to hold up to the sample preparation required for characterization. The instability of nanosheets formed from **17** may in part be due to the low hydrophobicity of both the Nibu monomer (Figure 7, cLogP 0.83) and the overall peptoid chain as indicated by the short retention time (Figure 7k, 8.7 min). Even though the surface activity of **17** (Figure 7l, SP_{900} 22.8 ± 0.6 mN/m) is similar to that of **14**, the degree of hydrophobic interactions within the nanosheet core may be too weak to withstand mechanical stresses involved in sample preparation.

Importantly, these results show that aromatic interactions within the hydrophobic core are not required for the formation of nanosheets. In particular, only the peptoids with the branched aliphatic monomers formed nanosheets. Brief studies were also performed on block-charge 36-residue peptoids in which the hydrophobic monomers contained straight-chain aliphatic groups ranging from 5 to 8 carbons, the details of which are discussed in the Supporting Information (Figure S12). For these peptoids, only a few small nanosheets were formed. These studies further demonstrate that including branched aliphatic monomers in peptoids is likely necessary for forming nanosheets that lack an aromatic core.

CONCLUSIONS

A systematic approach to evaluate a series of peptoid structures for assembly into nanosheets has provided some basic design rules for the types of hydrophobic monomers that can be tolerated in nanosheet formation. A variety of commercially available hydrophobic monomers were readily incorporated into peptoid sequences and were evaluated for the formation of stable nanosheets. We found that the aromatic ring of the Npe monomer can be substituted with hydrophobic moieties at the para and meta positions but not at the ortho position. In addition, we discovered that aromatic rings are not required to form a stable nanosheet and that branched aliphatic monomers are reasonably well tolerated.

The ability to adsorb to the air−water interface, as measured by the magnitude of the SP_{900} values, was not a good predictor of nanosheet formation yet did serve as a good indicator of peptoids that were above their critical aggregation concentration. The positioning of a methyl substituent on the aromatic ring played a significant role in whether the peptoids were above their critical aggregation concentration, with para substitution resulting in peptoids that were prone to aggregation. Peptoid conformational flexibility was found to likely to play a significant role in the ability of peptoids to form stable nanosheets, in that nanosheet formation was prevented when aromatic or aliphatic rings were directly attached to the peptoid backbone. DKP crystal structures, which were used as model compounds to examine the lateral packing density of substituted Npe monomers within the nanosheet hydrophobic core, showed that the closer the aromatic rings could pack together, the more successful the analogues were in forming nanosheets. These results suggest that peptoids with substitution at the ortho position of the Npe aromatic ring may be sterically hindered from forming stable nanosheets. Because many of the peptoids that did not form nanosheets were still able to adsorb to the air−water interface, we conclude that the viscoelastic behavior of the peptoids, including the residence time of the peptoid chains within the monolayer before collapse, must play a key role in whether a specific peptoid sequence will form a nanosheet.[34] This study demonstrates that the nanosheet structure is amenable to substantial chemical modification and provides a roadmap as to where new functionality can be introduced.

ASSOCIATED CONTENT

Supporting Information

The Supporting Information is available free of charge on the ACS Publications website at DOI: 10.1021/acs.langmuir.6b02735.

Characterization data for peptoids **1**−**18**, HPLC traces for peptoids **1**−**18**, optical microscopy images of unrocked peptoids **1**−**18**, nanosheet stability studies, DKP crystal structures, characterization (SEM images, AFM images, and XRD spectrum) of peptoid nanosheets composed of **18**, peptoids with straight chain aliphatic hydrophobic monomers, and a nanosheet image gallery. (PDF)

JS-DKP-13dimethylphenyl crystal structure (CIF)

JJ-2-53-#6 crystal structure(CIF)

383_35 crystal structure (CIF)

0334-84-01 crystal structure (CIF)

0334-107-2 crystal structure (CIF)

0334-107-3 crystal structure (CIF)

0334-84-03 crystal structure (CIF)

AUTHOR INFORMATION

Corresponding Author

*E-mail: rnzuckerman@lbl.gov.

Notes

The authors declare no competing financial interest.

ACKNOWLEDGMENTS

This project was funded by the Defense Threat Reduction Agency under contract no. DTRA10027-15875 and the DARPA Fold F(x) program. The work was conducted at the Molecular Foundry with support from the Advanced Light Source at Lawrence Berkeley National Laboratory, both of which are supported by the Office of Science, Office of Basic Energy Sciences, U.S. Department of Energy under contract no. DEAC02-05CH11231. Crystallographic data was obtained by

DOI: 10.1021/acs.langmuir.6b02735
Langmuir XXXX, XXX, XXX−XXX

Dr. Antonio G. DiPasquale at UC Berkeley's Small Molecule X-ray Crystallography Facility. C.P. is grateful for a postdoctoral fellowship from the Natural Sciences and Engineering Council of Canada (NSERC).

REFERENCES

(1) Govindaraju, T.; Avinash, M. B. Two-Dimensional Nanoarchitectonics: Organic and Hybrid Materials. *Nanoscale* **2012**, *4*, 6102−6117.
(2) Lau, K. H. A. Peptoids for Biomaterials Science. *Biomater. Sci.* **2014**, *2*, 627−633.
(3) Zhuang, X.; Mai, Y.; Wu, D.; Zhang, F.; Feng, X. Two-Dimensional Soft Nanomaterials: A Fascinating World of Materials. *Adv. Mater.* **2015**, *27*, 403−427.
(4) Butler, S. Z.; Hollen, S. M.; Cao, L.; Cui, Y.; Gupta, J. A.; Gutiérrez, H. R.; Heinz, T. F.; Hong, S. S.; Huang, J.; Ismach, A. F.; Johnston-Halperin, E.; Kuno, M.; Plashnitsa, V. V.; Robinson, R. D.; Ruoff, R. S.; Salahuddin, S.; Shan, J.; Shi, L.; Spencer, M. G.; Terrones, M.; Windl, W.; Goldberger, J. E. Progress, Challenges, and Opportunities in Two-Dimensional Materials Beyond Graphene. *ACS Nano* **2013**, *7*, 2898−2926.
(5) Colson, J. W.; Dichtel, W. R. Rationally Synthesized Two-Dimensional Polymers. *Nat. Chem.* **2013**, *5*, 453−465.
(6) Sakamoto, J.; van Heijst, J.; Lukin, O.; Schluter, A. D. Two-Dimensional Polymers: Just a Dream of Synthetic Chemists? *Angew. Chem., Int. Ed.* **2009**, *48*, 1030−1069.
(7) Ariga, K.; Malgras, V.; Ji, Q.; Zakaria, M. B.; Yamauchi, Y. Coordination Nanoarchitectonics at Interfaces between Supramolecular and Materials Chemistry. *Coord. Chem. Rev.* **2016**, *320*−*321*, 139−152.
(8) Fujie, T. Development of Free-Standing Polymer Nanosheets for Advanced Medical and Health-Care Applications. *Polym. J.* **2016**, *48*, 773−780.
(9) Whittell, G. R.; Hager, M. D.; Schubert, U. S.; Manners, I. Functional Soft Materials from Metallopolymers and Metallosupramolecular Polymers. *Nat. Mater.* **2011**, *10*, 176−188.
(10) Zhiyong, T.; Kotov, N. A.; Magonov, S.; Ozturk, B. Nanostructured Artificial Nacre. *Nat. Mater.* **2003**, *2*, 413−418.
(11) Mándity, I. M.; Fülöp, F. An Overview of Peptide and Peptoid Foldamers in Medicinal Chemistry. *Expert Opin. Drug Discovery* **2015**, *10*, 1163−1177.
(12) Yoo, B.; Shin, S. B. Y.; Huang, M. L.; Kirshenbaum, K. Peptoid Macrocycles: Making the Rounds with Peptidomimetic Oligomers. *Chem. - Eur. J.* **2010**, *16*, 5528−5537.
(13) Park, S.; Kwon, Y.-U. Facile Solid-Phase Parallel Synthesis of Linear and Cyclic Peptoids for Comparative Studies of Biological Activity. *ACS Comb. Sci.* **2015**, *17*, 196−201.
(14) Lee, J. H.; Meyer, A. M.; Lim, H.-S. A Simple Strategy for the Construction of Combinatorial Cyclic Peptoid Libraries. *Chem. Commun.* **2010**, *46*, 8615−8617.
(15) Holub, J. M.; Jang, H.; Kirshenbaum, K. Fit to Be Tied: Conformation-Directed Macrocyclization of Peptoid Foldamers. *Org. Lett.* **2007**, *9*, 3275−3278.
(16) Shah, N. H.; Butterfoss, G. L.; Nguyen, K.; Yoo, B.; Bonneau, R.; Rabenstein, D. L.; Kirshenbaum, K. Oligo(N-Aryl Glycines): A New Twist on Structured Peptoids. *J. Am. Chem. Soc.* **2008**, *130*, 16622−16632.
(17) Shin, S. B. Y.; Yoo, B.; Todaro, L. J.; Kirshenbaum, K. Cyclic Peptoids. *J. Am. Chem. Soc.* **2007**, *129*, 3218−3225.
(18) Stringer, J. R.; Crapster, J. A.; Guzei, I. A.; Blackwell, H. E. Extraordinarily Robust Polyproline Type I Peptoid Helices Generated Via the Incorporation of Alpha-Chiral Aromatic N-1-Naphthylethyl Side Chains. *J. Am. Chem. Soc.* **2011**, *133*, 15559−15567.
(19) Gangloff, N.; Ulbricht, J.; Lorson, T.; Schlaad, H.; Luxenhofer, R. Peptoids and Polypeptoids at the Frontier of Supra- and Macromolecular Engineering. *Chem. Rev.* **2016**, *116*, 1753−1802.
(20) Robertson, E. J.; Battigelli, A.; Proulx, C.; Mannige, R. V.; Haxton, T. K.; Yun, L.; Whitelam, S.; Zuckermann, R. N. Design, Synthesis, Assembly, and Engineering of Peptoid Nanosheets. *Acc. Chem. Res.* **2016**, *49*, 379−389.
(21) Olivier, G. K.; Cho, A.; Sanii, B.; Connolly, M. D.; Tran, H.; Zuckermann, R. N. Antibody-Mimetic Peptoid Nanosheets for Molecular Recognition. *ACS Nano* **2013**, *7*, 9276−9286.
(22) Flood, D.; Proulx, C.; Robertson, E. J.; Battigelli, A.; Wang, S.; Schwartzberg, A. M.; Zuckermann, R. N. Improved Chemical and Mechanical Stability of Peptoid Nanosheets by Photo-Crosslinking the Hydrophobic Core. *Chem. Commun.* **2016**, *52*, 4753−4756.
(23) Bornscheuer, U. T.; Huisman, G. W.; Kazlauskas, R. J.; Lutz, S.; Moore, J. C.; Robins, K. Engineering the Third Wave of Biocatalysis. *Nature* **2012**, *485*, 185−194.
(24) Moll, D.; Huber, C.; Schlegel, B.; Pum, D.; Sleytr, U. B.; Sara, M. S-Layer-Streptavidin Fusion Proteins as Template for Nanopatterned Molecular Arrays. *Proc. Natl. Acad. Sci. U. S. A.* **2002**, *99*, 14646−14651.
(25) Mannige, R. V.; Haxton, T. K.; Proulx, C.; Robertson, E. J.; Battigelli, A.; Butterfoss, G. L.; Zuckermann, R. N.; Whitelam, S. Novel Secondary Structure of Biomimetic Polymers Enables Extended Two-Dimensional Assemblies. *Nature* **2015**, *526*, 415−420.
(26) Proulx, C.; Yoo, S.; Connolly, M. D.; Zuckermann, R. N. Accelerated Submonomer Solid-Phase Synthesis of Peptoids Incorporating Multiple Substituted N-Aryl Glycine Monomers. *J. Org. Chem.* **2015**, *80*, 10490−10497.
(27) http://www.molinspiration.com.
(28) Sanii, B.; Kudirka, R.; Cho, A.; Venkateswaran, N.; Olivier, G. K.; Olson, A. M.; Tran, H.; Harada, R. M.; Tan, L.; Zuckermann, R. N. Shaken, Not Stirred: Collapsing a Peptoid Monolayer to Produce Free-Floating, Stable Nanosheets. *J. Am. Chem. Soc.* **2011**, *133*, 20808−20815.
(29) Ravera, F.; Loglio, G.; Kovalchuk, V. I. Interfacial Dilational Rheology by Oscillating Bubble/Drop Methods. *Curr. Opin. Colloid Interface Sci.* **2010**, *15*, 217−228.
(30) Borthwick, A. D. 2,5-Diketopiperazines: Synthesis, Reactions, Medicinal Chemistry, and Bioactive Natural Products. *Chem. Rev.* **2012**, *112*, 3641−3716.
(31) Murnen, H. K.; Rosales, A. M.; Jaworski, J. N.; Segalman, R. A.; Zuckermann, R. N. Hierarchical Self-Assembly of a Biomimetic Diblock Copolypeptoid into Homochiral Super Helices. *J. Am. Chem. Soc.* **2010**, *132*, 16112−16119.
(32) Rosen, M. J. Adsorption of Surface-Active Agents at Interfaces: The Electrical Double Layer. *Surface and Interfacial Phenomena*, 3rd ed.; Wiley-Interscience: Hoboken, NJ, 2004; pp 34−104.
(33) Nam, K. T.; Shelby, S. A.; Choi, P. H.; Marciel, A. B.; Chen, R.; Tan, L.; Chu, T. K.; Mesch, R. A.; Lee, B.-C.; Connolly, M. D.; Kisielowski, C.; Zuckermann, R. N. Free-Floating Ultrathin Two-Dimensional Crystals from Sequence-Specific Peptoid Polymers. *Nat. Mater.* **2010**, *9*, 454−460.
(34) Robertson, E. J.; Nehls, E. M.; Zuckermann, R. N. Structure-Rheology Relationship in Nanosheet-Forming Peptoid Monolayers. *Langmuir* **2016**, DOI: 10.1021/acs.langmuir.6b02736.
(35) Krylov, D.; Vinson, C. R. Leucine Zipper. *eLS*; John Wiley & Sons, Ltd, 2001; DOI: 10.1038/npg.els.0003001.

DOI: 10.1021/acs.langmuir.6b02735
Langmuir XXXX, XXX, XXX−XXX